Fatigue life and initiation mechanisms in wrought Inconel 718 DA for different microstructures

Meriem Abikchi[1,2,*], Thomas Billot[3], Jerome Crepin[1], Arnaud Longuet[2], Caroline Mary[2], Thilo F. Morgeneyer[1], André Pineau[1]

[1] Mines ParisTech, Centre des Matériaux UMR CNRS 7633, BP 87, 91003 Evry cedex, France
[2] Snecma-SAFRAN group ; site de Villaroche, 77550 Moissy-Cramayel, France
[3] Snecma-SAFRAN group ; site de Gennevilliers, 92702 Colombes Cedex, France

* Corresponding author: meriem.abikchi@mines-paristech.fr

Abstract Wrought Inconel 718 DA superalloy disk zones present a wide range of behavior in fatigue life due to the variability of the microstructure. In order to link the effect of the forging conditions and achieved microstructure to the fatigue life, two microstructures have been tested in fatigue. Fatigue tests under strain control were performed at 450°C. Grain size distributions and phase distributions were characterized in the specimens and related to fatigue failure initiation modes. Fatigue crack initiation was seen to occur on large grains in stage I for the larger grain material whereas for the material with slightly smaller grains initiation from internal nitrides caused failure via so-called fish-eye cracks. The different steps of these failure modes are discussed using data from the literature to gather the ingredients for a quantitative assessment of the fatigue lifetime using fracture mechanics.

Keywords Inconel 718, Microstructure, Fatigue, Crack initiation, Propagation mechanism

1. Introduction

Inconel 718 is widely used in aircraft industry. Because of a good combination of formability fatigue and weldability properties and low price/performance ratio, this superalloy is widely used for aerospace applications like turbine disks [1, 2]. This wrought material is produced by forging followed by different heat treatments in order to obtain the desired microstructure. The fatigue behavior at high temperature of this superalloy was widely studied [3-6], the main objective is to predict the lifetime of aircraft engine disk by calculation according to microstructures parameters [7, 8].

To improve the fatigue durability, it is important to obtain the finest possible microstructure. A specific heat treatment called Direct Aging (DA) was developed to obtain this kind of microstructure [9]. Contrary to a classical heat treatment, here the material is directly quenched after forging then aged without adding an annealing step. Fatigue tests were carried out on 718DA and even if the fatigue life was improved thanks to a finer grain size, a strong scatter in test results was observed [10]. Fractography revealed that this scatter is linked to different microstructures and crack initiation mechanisms [11]. Two mechanisms were identified, one for the fine grain size material (5-10µm) and another one for the large grain size material (150µm). For the fine microstructure, initiation sites were systematically related to the presence of second phase particles (carbides and nitrides) on the specimen surface with a size of 10-20µm, then Stage II crack propagation occurs until the breaking point. On the other hand, in the larger grain size material, conventional Stage I crack initiation was observed along the slip bands. In conclusion of this work [11], crack initiation always occurs in the larger microstructural phase. For the fine grain size material, it corresponds to the particles. When the grain size is larger than the particles, crack initiation occurs within the grains themselves. Also, in the previous study, the fatigue properties

were compared at 600°C, and strong oxidation effects are observed in particular on the NbC particles. This oxidation mechanism increases the volume of the particles and allows the initiation and propagation of local cracks because of stress concentration [9].
In the present study, the two materials which were investigated have a mean grain size smaller than the particles size because of the forging parameters used and the DA heat treatment. Two grain sizes were selected. In the case of small grain size the scatter of fatigue life is always present [10]. So it is necessary to understand which one of these parameters really affects the fatigue life.
In the present study the microstructural features are assessed via experimental observation methods. Mechanical fatigue tests are carried out and fatigue crack initiation mechanisms assessed via fractography observations. The various modes of crack initiation encountered and subsequent propagation are discussed using data from the literature to gather the ingredients for a quantitative assessment of the contributions of each crack progression step on the fatigue lifetime.

2. Materials and experimental methods

The experimental pancakes used in this study were forged by Snecma. The pancakes, which were water quenched after forging, have been directly aged with the standard aging treatment, and will be designated as DA718 in the following. The standard aging treatment is: 720°C /8h/ Furnace cooling (50°C/h) down to 620°C/8h and subsequent air cooling. In the present study, two kinds of forging parameters have been investigated (such as temperature, strain amplitude or cooling speed). Indeed material 1 presents a cooling speed slower, as well as a hold time at temperature higher than the delta phase solvus temperature longer than the material 2.

Inconel 718 is a nickel based superalloy hardened by γ'' (Ni_3Nb) and γ' ($Ni_3[Ti,Al]$) precipitates. This alloy also contains δ (Ni_3Nb) phase. The δ phase particles are located both along the grain boundaries and within the grains, depending on the heat treatment applied to the alloy. Another category of coarse second phase particles present in the alloy are nitrides (TiN) and carbides (NbC) with a typical size ranging from 5 to 20 μm. These particles are preferentially located at grain boundaries [14].

Table 1 : Chemical composition of Inconel 718 in weigth %

Al	B	C	Cr	Co	Cu	Fe	Mn	Mo	Ni	Nb+Ta	Ti	O	N
0.56	0.0041	0.023	17.97	0.14	0.03	17.31	0.08	2.97	54.18	5.40	1.00	0.001	0.0062

Microstructures were assessed in term of grain size, particle (carbides and nitrides) and δ phase sizes and their distributions. Samples were polished up to 1μm diamond paste. Micrographs of these samples were taken using a Scanning Electron Microscope (SEM), LEO VP 1450 SEM. To measure precipitates and particles size and their distributions, image analysis software, ImageJ®, was used.
Electron back scatter diffraction (EBSD) scans were also carried out on polished samples. EBSD patterns were collected using a Hikari digital camera, installed on a LEO SEM system. LEO VP 1450 SEM is equipped with an EDAX TSL OIM EBSD data acquisition and processing software and a Hikari digital camera. Operating conditions: high voltage 30 kV, probe current 2000 pA, working distance 22.5 mm, tilt angle 70 deg, step size 0.5 micrometers (hexagonal grid). Four areas of 500μm² were scanned on each material. Data cleanup by "Grain dilation" with threshold values of grain size and misorientation angle of 2 pixels and 5 degrees, respectively.
All the mechanical tests were performed on specimens taken from the two forged material which were submitted to DA heat treatment. The specimens were oriented along the tangential direction of the pancakes.
Fatigue tests were performed using a servo-hydraulic MTS testing machine with a maximum loading of 250kN. This machine was equipped with a resistance heating furnace allowing a

maximum temperature of 1200°C. The fatigue tests were carried out in air at 450 °C ± 2 °C. The temperature control was realized with thermocouple welded on each head of the sample surface (outside the gauge length). These specimens had a diameter of 5 mm and a gauge length of 13 mm. The specimens were tested under 1Hz triangular cycles under strain control. SEM observations of the fracture surfaces allowed us to identify the nature of the fatigue crack initiation sites using a Zeiss Gemini SEM.

3. Results and discussion

3.1. Microstructure

Figure 1 shows EBSD data for the two materials. Differences in grain size are observed. In material 1, the average size of grains is about 10µm whereas it is only about 7µm in material 2. The distribution of the grain size is also different (Figure 2); the scatter of the distribution of grain size is larger in material 1. EBSD data also show that both materials do not have a preferred crystal orientation (i.e. texture in Figure 3).

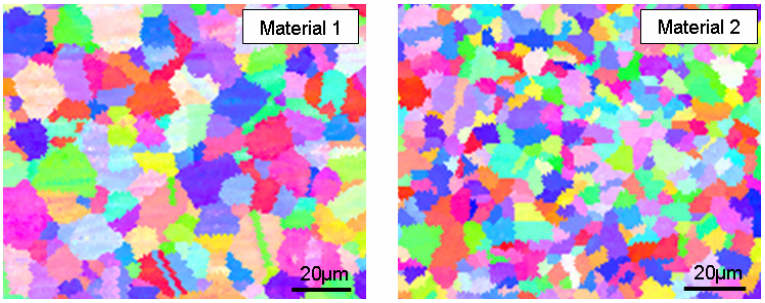

Figure 1 : Grain microstructures observed by EBSD scans with a step of 0.5 µm for a) material 1 and b) material 2

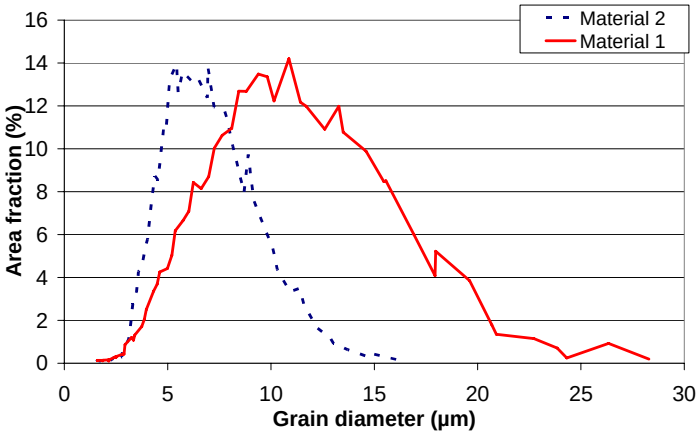

Figure 2 : Grain size distributions of the 2 materials calculated from the EBSD data on 1mm² zones

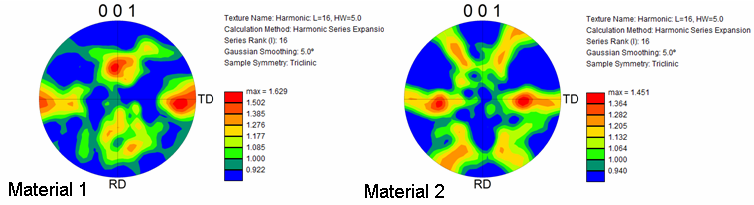

Figure 3 : Pole figure of the texture of the two materials

The size and the distribution of the particles (carbides and nitrides) were also determined by SEM observations on cut-sections first (Figure 4). Carbides are bigger in the initial, non-wrought material

than in the wrought materials, which is consistent with the fact that the carbides were “cut” during the forging process (Table 2). During forging, clusters of smaller carbides are formed that are oriented according to the fibre direction. These results were obtained from a 1mm² surface.

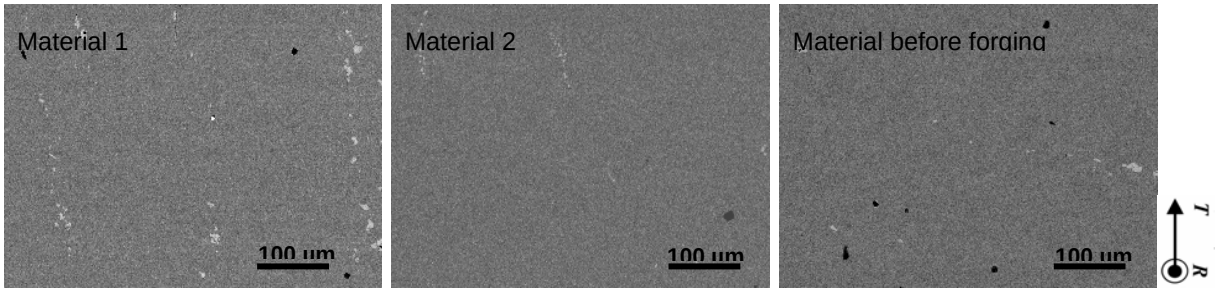

Figure 4 : Microstructures of the different materials, comparison of the distribution of carbides and nitrides, in the radial direction.

Table 2 : Comparison of the distribution and the size of the carbides in the three materials, analysis zones of 1mm².

	Numbers of carbides	Average size	Average diameter	Maximal size	Maximal diameter
	(±5)	µm² (±0,5)	µm	µm² (±0,5)	µm
Material 1	185	13.3	6.5	139.0	20.9
Material 2	115	16.9	7.3	121.5	19.5
Material before forging	95	25.6	9.0	220.5	26.3

The same analysis was carried out for the nitrides which are particles with sharper angles than the carbides (Figure 4). Their density seems similar in both materials, only their size differs weakly. To carry this study further, and compare the distribution of the nitrides in the two materials, a larger area of analyses should be used to assess enough particles for a statistical study.

Table 3 : Comparison of the distribution and the size of the nitrides in the three materials, analyse zones of 1mm².

	Numbers of nitrides	Average size	Average diameter	Maximal size	Maximal diameter
	(±5)	µm² (±0,5)	µm	µm² (±0,5)	µm
Material 1	23	33.3	10.2	204.1	25.3
Material 2	24	27.2	9.2	154.9	22.1
Material before forging	22	17.9	7.5	101.0	17.8

The last microstructural comparison concerns the proportion of δ phase in the two materials of the study (Figure 5). The fraction of δ phase is three times higher in material 2 compared to material 1; they are respectively of 3.0% and 1.1%. This δ phase precipitates preferentially on grain boundaries.

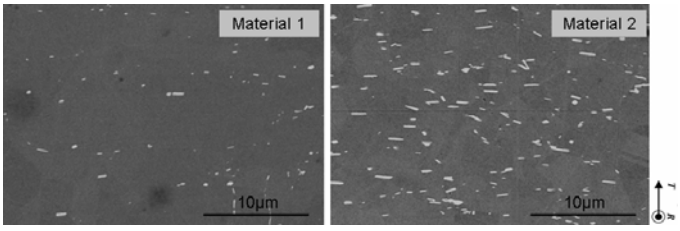

Figure 5 : Comparison of the delta phase distribution between the two materials.

3.2. Mechanical test results

The difference of yield stress between the material 1 and 2 is observed; they are respectively 1170 MPa and 1250MPa. Fatigue properties of these two materials are compared in relation with the grain sizes. The results are presented in Figure 6, the pseudo-stress values are normalised by the Young modulus divided by the mean yield stress of the material, and for proprietary reason this

value cannot be indicated. As shown in Figure 6, for tests conducted at 450°C, the small grain size material achieves significantly higher fatigue lives than the larger grain size material. The fatigue life of material 2 is at least twice superior to that of the material 1.

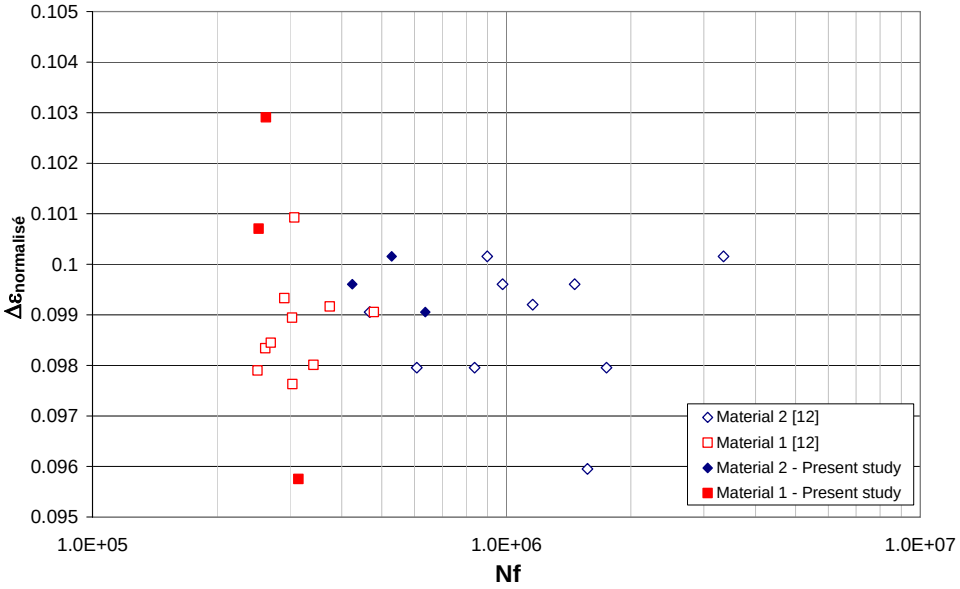

Figure 6 : Repartition of the fatigue life at 450°C, Comparison of the two microstructures**.**

3.3. Discussion of the fatigue crack initiation scenarios and crack propagation steps

In this section the different crack initiation and propagation scenarios are discussed in detail and compared with the literature to gather the elements necessary for a quantitative study of the contribution of each crack progression mechanism to the total fatigue lifetime.

Inconel 718 DA presents at least two known modes of crack initiation [9, 11] modes depending of the microstructure for smooth round bars:
1. Crack initiation on the surface particles for the lowest fatigue life
2. Stage I crack initiation for the longest fatigue life.
In this study, a supplementary crack initiation mode is observed:
3. Internal crack initiation on nitrides leading to fish-eye cracks.
This third crack initiation mode appears for long fatigue lifes and will be discussed in detail.

3.3.1. Crack initiation on surface particle

This type of fatigue crack initiation phenomenon is not shown here but it was clearly observed in the F. Alexandre's work [9, 11] for larger strain amplitude and temperature. These brittle particles may fracture during loading. In addition, the niobium carbides particles on the surface are strongly oxidized and transformed into Nb_2O_5 type oxide [9, 15], as shown in Figure 7. The increased volume of carbides and the stress concentration associated with the oxidation of carbides may lead to early crack initiation. The surface crack initiation probability is dependent of the probability to encounter a large oxidized particle on the specimen surface. This probability increases for large specimens. The fatigue life is then mainly spent in Stage II propagation from an initial crack size equal to the size of the larger grain.

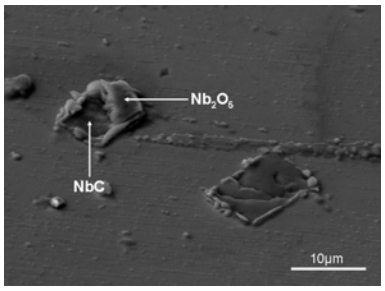

Figure 7 : SEM micrograph of the outer specimen surface away from the fracture surface after specimen failure; oxidized carbides surrounding nitrides are seen

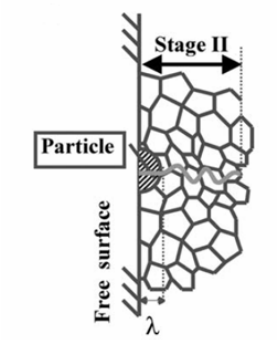

Figure 8 : Schematic representation of the fracture mechanisms for crack initiation from a surface particle [11]

3.3.2. Stage I crack initiation on large grains via persistent slip bands (PSB)

For the larger grain size material 1, the fatigue crack initiation corresponded to typical Stage I crack initiation along persistent slip bands as shown in Figure 9 for two specimens. The stage I crack initiation takes place over several grains, it occurs from the larger grains of material 1. This type of crack initiation was already observed in a previous study [9, 11] for larger mean grain size material, about 50µm.

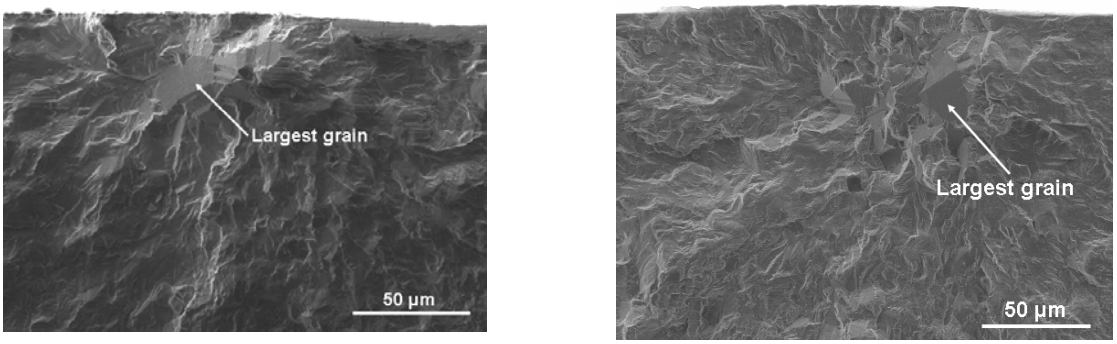

Figure 9 : Fatigue crack initiation sites on microstructure 1 with the biggest mean grains size (11 µm) : Stage I crack initiation across an area of several grains of (a) 70µm of diameter and (b) 150µm of diameter

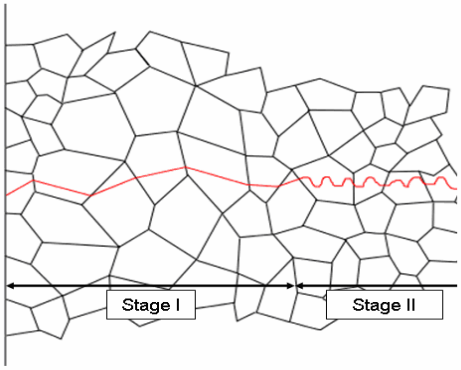

Figure 10 : Schematic representation of the fatigue crack initiation and propagation mechanisms for stage I initiation (for the material with larger grains in the present study)

A probabilistic life model was described by F. Alexandre [11] for this mechanism. The number of crack initiation cycles has been assessed using a Tanaka-Mura [16] type formulation with a modification to account for grain size effect.

$$N_i = \frac{1}{d}\frac{A_{StageI}}{(\Delta\varepsilon_p)^2} \quad (1)$$

where N_i is the number of cycles to initiation, d is the grain size (here, 7µm), $\Delta\varepsilon_p$ is the strain plastic amplitude (in our study, the macroscopic plastic strain is almost equal to zero), and A_{stageI} a constant depending on temperature. This model accounting for grain size effect is consistent with the findings of our study because crack initiation occurs on the largest grains for the material with the larger grains.
This stage I crack initiation is known to be sensitive to the size of the γ'' precipitates [17]. Indeed the γ'' precipitates influence the homogenization on the slip bands. Reducing the risk of crack initiation via PSBs [18].When the grain size is small, the size of the γ'' precipitates increases and the slip bands are more homogeneously distributed in the grains. So this theory may explain why stage I crack initiation occurs on the biggest grain of the material. The dislocation structure and the precipitate size have an effect on the fatigue life [19].

3.3.3. Internal crack initiation on particles leading to a fish-eye crack

This last mechanism is observed in material 2 with smaller grains; crack initiation occurs on an internal particle (nitrides) leading to a fish-eye crack. The mechanism was widely observed for other materials, like in steels for very cycle fatigue [20, 21]. Only a semi-quantitative discussion of crack initiation and propagation steps is presented here.

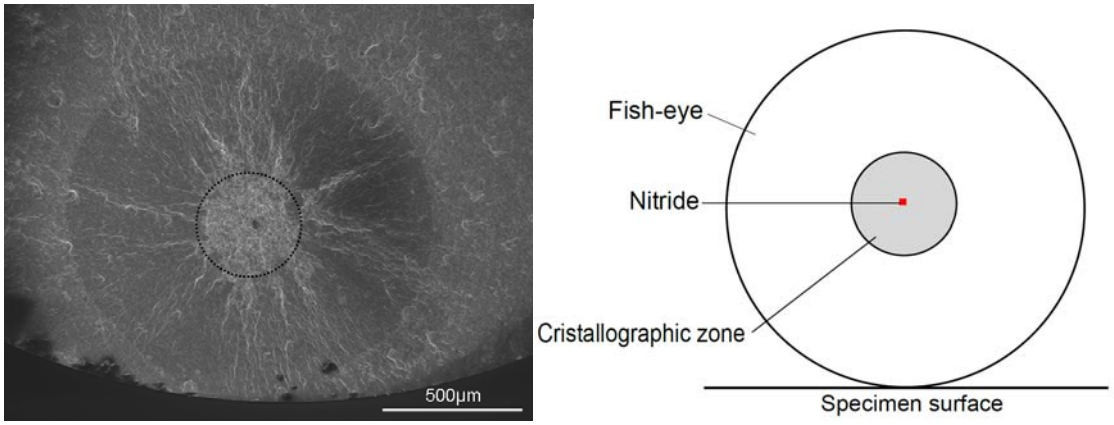

Figure 11 : SEM micrography of a fish-eye crack with a dark nitride particle in its centre for the small grain material 2 and the schematic representation

SEM observations (Figure 11) show an example of a fish-eye pattern formed on the fracture surface and the nitride at the centre of the fish eye. The difference of contrast between the three zones observed on the fracture surface suggests different crack growth mechanisms. At the centre of the fish-eye mark, a bright-facet area was found around the inclusion at the fracture origin as shown in Figure 12. The bright-facet area reveals a very rough topology compared to the area inside the fish-eye.
The propagation mechanism can be classified in five steps:

I. fracture of the large nitride during loading (or during forging)
II. Near threshold micropropagation with crystallographic character, under vacuum
III. vacuum stage II propagation (few striations),
IV. Air propagation with marked striations when the crack reaches specimen surface,
V. final ductile fracture

All these steps will be studied to gather elements to better understand the contribution of the

fracture phenomena on fatigue life.

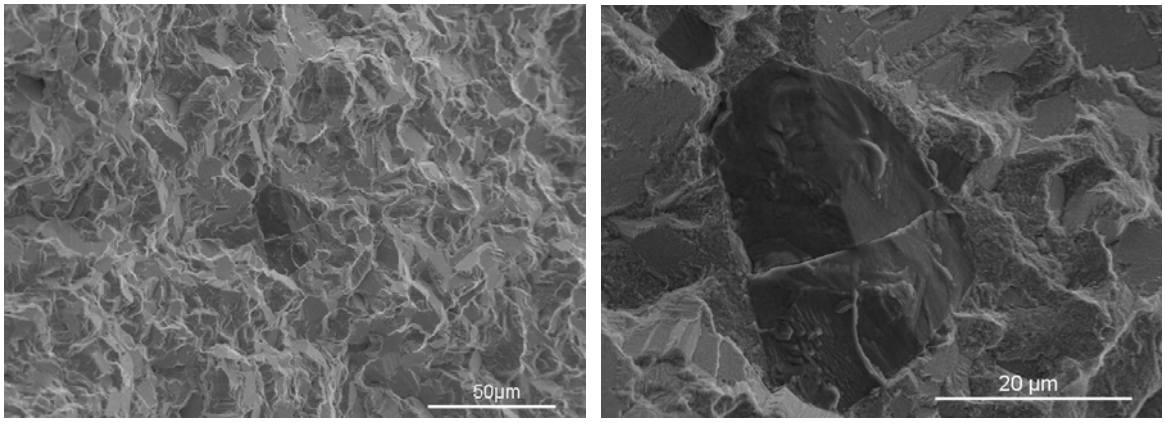

Figure 12 : SEM micrograph showing a zoom in the centre of the fish-eye crack displaying the fractured nitride particle and the rough micro-propagation with crystallographic character

I. Large nitride broken during loading (or during forging)

The nitride cracking is dependent on the particle size and applied stress [9, 11]. As a consequence the distribution of the nitrides through the material plays a role on the fatigue life of a structure. The crack initiation always occurred on the largest nitrides for the present study when comparing according to surface characterization of the nitrides distribution realised (Table 3).

II. Vacuum near threshold micropropagation with crystallographic character

The question is if a cracked nitride leads to crack propagation from the first load cycle onwards. If the value of stress intensity factor generated by the cracked nitride is superior to the threshold value this will be the case. Based on the size of the particles found in the crack initiation site, the initial stress intensity factor range, $\Delta K_{ini,}$ can calculated for a penny shaped crack in a cylinder using the following formula [22]:

$$\Delta K_{ini,inclusion} = 0{,}5\,\sigma_a\,\sqrt{\pi\sqrt{area_{inclusion}}} \qquad (2)$$

Where, σ_a is the stress amplitude. The initial stress intensity factor calculated from a nitride size is between 4MPa√m and 6MPa√m for different specimens displaying internal crack initiation. According to Lawless and King's studies [23, 24], the stress intensity threshold in air for 718 DA, at 538°C and 550°C respectively, is about 8MPa√m. At 427°C in air [19] the threshold for a fine microstructure varies between 5MPa√m and 9MPa√m depending of the heat treatment and the stress ratio. This threshold decreases when the grain size decreases [19, 23]. These values have been found for crack propagation in air; the initiation of the internal fish eye crack occurs, however, in vacuum. Few studies about propagation threshold were performed in vacuum. In [25] the threshold seems to be closed from the one in air when extrapolating the given curve. Material 2 of this study has a small mean grain size (about 7µm) which can reduce the propagation threshold. In addition the residual stress around the particle may be in tension and lead to an effective stress intensity factor which is higher than the one calculated here which would facilitate the propagation.

Furthermore most the threshold values given in the literature have been obtained for long cracks. However, for the fish eye crack initiation, the initial crack is the cracked nitride which is a short crack. It may be assumed that due to the short crack behavior crack progression may occur below threshold values obtained for long cracks [26].

The last parameter which can influence the initial stress intensity factor is the shape of the particle. The corners of the cubic nitrides may generate a stress intensity factor that is superior to the one obtained by the equation (2) for a penny shaped crack

The propagation speed and consequently the fatigue life of this step is certainly low because of the

roughness of the crystallographic surface [1, 13]

III. Vacuum stage II propagation (little striations)

The second area inside the fish-eye presents a classic stage II fracture surface, but the striations are not marked. This can be explained by the fact that this propagation step still occurs in vacuum [13]. Utilisation of Pedron's data [25] is certainly suitable in this step of the propagation. This step propagation stops when the crack reaches the specimen surface.

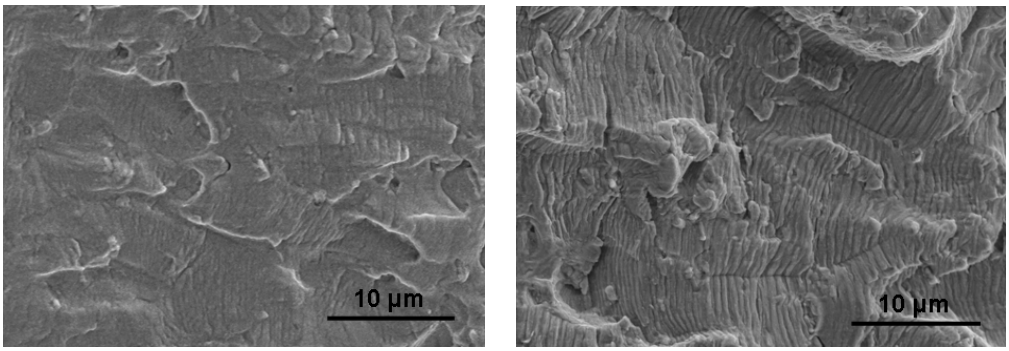

Figure 13 : SEM fractography of the stage II fatigue a) vacuum crack propagation in the fish eye b) air crack propagation beyond the fish-eye.

IV. Crack reaches specimen surface air propagation with marked striations

When the fish-eye crack reaches the specimen surface, the ligament between the penny-shaped fish-eye crack and the specimen surface will break very quickly due to the high local stress intensity factor.

In this step the surface crack can approximately be considered as semi-elliptical. The propagation occurs in air:

$$K = \sigma\sqrt{\pi d}\ F_I \quad (3)$$

Where σ is applied stress, *d* the crack depth from the surface and F_I the correction factor depending on the geometry of the specimen and crack. Values of this factor F_I can be found in handbooks [22]. The last step on the fracture mode corresponds to final ductile fracture.

In conclusion, 3 different crack initiation scenarios have been identified for Inconel 718. The likelihood of the occurrence of each of these scenarios depends on the microstructural heterogeneities, such as e.g. grain size distributions, particle size distributions and their spatial distributions. The link between the probability to encounter each crack initiation scenario and the total fatigue life of the specimens is schematically sketched in **Figure 14**. Further analysis of the resulting distributions in fatigue life is under progress.

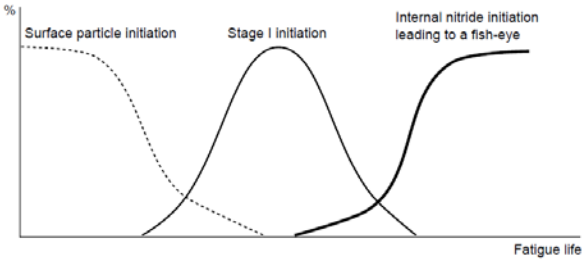

Figure 14 : Schematic representation of the relationship between probability to encounter each crack initiation scenario function with the total fatigue life of the specimen for a specific loading value (the relative position of the stage I initiation curve and the internal nitride initiation curve is dependent of a scale effect. These curves can be translated.)

Conclusions

The differences in fatigue life behavior in Inconel 718DA are studied here for two different microstructures. In both microstructures of the present study, the average grain size is smaller than the particle (nitrides) size and nevertheless crack initiation sites are different. In the larger (10μm) grain size material, stage I crystallographic cracking at or near the surface is initiated on the large grains of the material located at the free surface and having a diameter about 30 μm. In small (7μm) grain size material, crack initiation occurs preferentially on internal TiN particles followed by crack propagation with crystallographic character and subsequent Stage II crack propagation. A fish-eye crack is formed. The particles initiating the internal fatigue cracks are substantively larger than the largest particles observed on cut section from microstructural analyses. The internal crack occurs on nitrides of a mean diameter of 30μm. The different stages of the fish eye cracks are identified with: I. fracture of the large nitride during loading (or during forging), II. vacuum near threshold micropropagation with crystallographic character, III.vacuum stage II propagation (few striations), IV.crack reaches the specimen free surface, and propagation in air with marked striations and V.final ductile fracture. These crack progression stages are discussed using data from the literature to gather elements for quantitative assessment of the contribution of each crack progression step to the total specimen lifetime.

Acknowledgements

Snecma, Safran group, is gratefully acknowledged for financial support and material provision.

References

[1] C. Bathias, A. Pineau, Fatigue des Matériaux et des Structures 3, Hermes science publication, (2009).

[2] D. F. Paulinis, J.J. Schirra, Alloy 718 at Pratt & Whitney – Historical perspective and future challenges, Superalloys 718, 625, 706 and derivatives, ed. by E. E. Loria, TMS, (2001).

[3] R. L. Saha, K. Gopinath, K. K. Sharma and M. Srinivas, Low cycle fatigue behaviour of alloy 718 disc forging at elevated temperatures, Superalloys 718, 625, 706 and derivatives, ed. by E. E. Loria, TMS, (2001).

[4] W. L. Mills and C. M. Brown, Fatigue fracture surface morphology for alloy 718, Superalloys 718, 625, 706 and derivatives, ed. by E. E. Loria, TMS, (2001).

[5] J. Warren, D.Y. Wei, The cyclic fatigue behaviour of direct aged 718 at 149, 315, 454 and 538 °C, Materials Science and Engineering A 428, 106-115, (2006).

[6] S. P. Lynch, T. C. Radtke, B. J. Wicks and R. T. Byrnes, Fatigue crack growth in nickel-based superalloys at 500-700°C. II: Direct aged alloy 718, Fatigue Fract. Engng Mater. Struct. Vol. 17, No. 3, pp. 313-325, (1994).

[7] S. Deyber, F. Alexandre, J. Vaissaud and A. Pineau, Probabilistic life of DA718 for aircraft engine disks, Superalloys 718, 625, 706 and derivatives, ed. by E. E. Loria, TMS, (2005).

[8] M. Stoschka, M. Stockinger, H.Maderbacher and M. Riedler, A closed concept to associate the hot-forging process controlled microstructure with fatigue life, Proceedings Superalloys 2012, TMS, (2012).

[9] F. Alexandre, Probabilistic and microstructural aspect of fatigue crack initiation in IN718, PhD thesis, Ecole des mines de Paris, (2004).

[10] V. Zerrouki, Inconel 718 et tenue en fatigue oligocyclique. Influence de la microstructure et prédiction de la durée de vie, Mémoire de DRT Génie des Matériaux, université EVRY, (2000)

[11] F. Alexandre, S. Deyber, A. Pineau, Modelling the optimum grain size on the low cycle fatigue of a Ni based seperalloy in the presence of two possible crack initiation sites, Scripta Materialia, 50, pp. 25-30, (2004),.

[12] Y. Desvallèes, M. Bouzidi, F. Bois, N. Beaude, Delta phase in Inconel 718 : Mechanical

properties and forging process requirements, Superalloys 718, 625, 706 and various derivatives, (1994).
[13] S. Suresh, Fatigue of Materials Second Edition, Cambridge University Press, (1998).
[14] X. Huang et Al. Experimental investigations on microcrack initiation process in nickel-based superalloy DAGH4169. Int J Fatigue (2011).
[15] T. Connolley, P. A. S. Reed, J. M. Starink, Short crack initiation and growth at 600°C in notched specimens of Inconel 718, Materials Science and Engineering, A340 1-2, pp. 139-154, (2003).
[16] K. Tanaka and T. Mura, A dislocation model for fatigue crack initiation, journal of Applied Machanics, Vol.48, pp. 97-103, (1981),
[17] Effect of Direct Aging on the microstructure and the mechanical properties of Alloy 718 A.Devaux, L.Nazé, A.Organista, J.Y.Guédou, P. Héritier, In preparation.
[18] L. L. Li, P. Zhang, Z. J. Zhang, Z. F. Zhang, Effect of crystallographic orientation and grain boundary character on fatigue cracking behaviors of coaxial copper bicrystals, Acta Materialia 61, pp. 425-438, (2013).
[19] D. D. Krueger, Stephen D. Antolovich, and R. H. Van Stone, Effects of grain size and precipitate size on the fatigue crack growth behaviour of alloy 718 at 427°C, Metallurgical transactions A, Vol.18A, (1987)
[20] K. Shiozawa and L. Lu, Very high-cycle fatigue behaviour of shot-penned high-carbon-chromium bearing steel, Fatigue Fract Engng Mater Struct 25, pp. 813-822, (2002)
[21] T. Sakai, Y. Sato and N. Oguma, Characteristic S-N properties of high-carbon-chromium-bearing steel under axial loading in long-life fatigue, Fatigue Fract Engng Mater Struct 25, pp. 765-773, (2002).
[22] Y. Murakami, S. Kodoma and S. Konuma, Quantitative evaluation of effects of non-metallic inclusions on fatigue strength of high strength steel. Trans. JSME 54A, pp. 688-695, (1988)
[23] Bernard H. Lawless and A. W. Dix, Effect of processing/microstructure on threshold fatigue crack growth behaviour of alloy 718 forging, Superalloys 718, 625, 706 and various derivatives, (2001).
[24] J. E. King, Fatigue crack propagation in nikel-base superalloys – effects of the microstructure, load ratio and temperature, Materials science and technology, Vol.3, (1987).
[25] J. P. Pédron, A. Pineau, the effect of the microstructure and environment on the crack growth behaviour of inconel 718 alloy at 650°C under fatigue, creep and combined loading, Materials science and engineering, 56, pp. 143-156, (1982).
[26] A. Pineau, Short crack behavior in relation to three-dimensional aspects and crack closure effect, Small Fatigue Cracks. A publication of the Metallurgical Society, Inc. Warrendale, PA, (1986).